Vacuum-Evaporable Spin-Crossover Complexes in Direct Contact with a Solid Surface: Bismuth versus Gold

Sascha Ossinger,[†] Holger Naggert,[†] Lalminthang Kipgen,[‡] Torben Jasper-Toennies,[§] Abhishek Rai,[§] Julian Rudnik,[†] Fabian Nickel,[‡] Lucas M. Arruda,[‡] Matthias Bernien,[‡] Wolfgang Kuch,*[,‡] Richard Berndt,*[,§] and Felix Tuczek*[,†] [ID]

[†]Institut für Anorganische Chemie and [§]Institut für Experimentelle und Angewandte Physik, Christian-Albrechts-Universität zu Kiel, 24098 Kiel, Germany

[‡]Institut für Experimentalphysik, Freie Universität Berlin, Arnimallee 14, 14195 Berlin, Germany

S *Supporting Information*
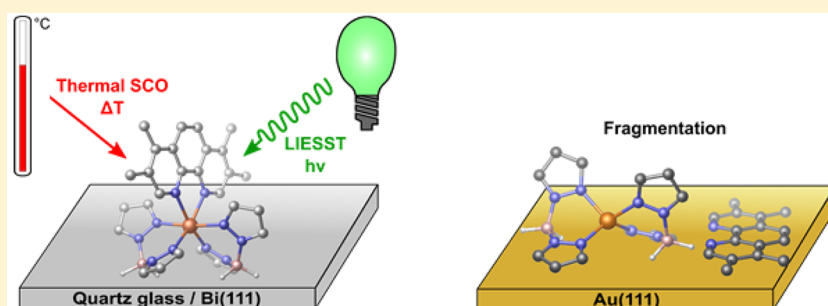
ABSTRACT: To investigate the ability for spin-state switching of spin-crossover (SCO) complexes adsorbed to solid substrates, the SCO complex $[Fe(H_2B(pz)_2)_2(phenme_4)]$ (pz = pyrazole, phenme$_4$ = 3,4,7,8-tetramethyl-1,10-phenanthroline) is prepared. The new complex is investigated by magnetic susceptibility measurements and Mößbauer spectroscopy in the solid state and by temperature-dependent UV/vis spectroscopy in a thin film deposited by physical vapor deposition (PVD) on quartz glass. Thermal- and light-induced SCO is observed in the bulk and the film on glass. Submonolayers of this complex obtained by PVD are studied by temperature-dependent near-edge X-ray absorption fine structure (NEXAFS) on Au(111) as well as Bi(111) and by scanning tunneling microscopy (STM) on Au(111). NEXAFS shows thermal- and light-induced spin-state switching of the complex on Bi(111), however, with a large temperature-independent high-spin fraction (~50%). On the other hand, combined evidence from NEXAFS and STM indicates that on Au(111) the complex dissociates into $[Fe(H_2B(pz)_2)_2]$ and phenme$_4$. Similar observations are made with the parent complex $[Fe(H_2B(pz)_2)_2(phen)]$, which on Bi(111) stays intact and exhibits thermal-induced as well as light-induced SCO, but on Au(111) dissociates into $[Fe(H_2B(pz)_2)_2]$ and phen.

INTRODUCTION

Spin-crossover (SCO) compounds of $3d^4-3d^7$ transition metals can be switched between two spin states and are promising building blocks for applications in spintronics, sensors, and data storage.[1-10] The preparation of high-quality molecular films of these compounds on a surface by physical vapor deposition (PVD) allows the control of thickness and morphology and can be fully integrated into thin-film-deposition techniques.[11-16] A prominent class of vacuum-evaporable SCO complexes are the compounds $[Fe(H_2B(pz)_2)_2(L)]$ (pz = pyrazole, L = 2,2'-bipyridine (bipy) or 1,10-phenanthroline (phen)).[9,14,17-22] Their iron(II) centers are coordinated by two monoanionic $H_2B(pz)_2$ ligands and a neutral coligand (phen or bipy). The transition from the paramagnetic ($S = 2$) high-spin (HS) state to the diamagnetic ($S = 0$) low-spin (LS) state can be induced by temperature, pressure, or light. Thermal- and light-induced spin-state switching in films of SCO complexes has been monitored by ultraviolet photoelectron spectroscopy, inverse photoemission,

and X-ray absorption spectroscopy (XAS) as well as scanning tunneling microscopy (STM).[9,23-30] In the course of these investigations it became evident that in direct contact with a Au(111) surface the complex $[Fe(H_2B(pz)_2)_2(phen)]$ (**1**) undergoes fragmentation to $[Fe(H_2B(pz)_2)_2]$ and 1,10-phenanthroline.[31] Keeping the gold substrate at elevated temperatures, however, it was observed that ordered mono-layers of intact molecules of **1** are formed which can be spin-switched by electron-induced excited spin-state trapping (ELIESST).[9] Nevertheless, in less dense regions of these layers phenanthroline molecules from decomposed **1** were still visible.[31]

Replacing the gold substrate by highly oriented pyrolytic graphite (HOPG), no decomposition of $[Fe(H_2B(pz)_2)_2(phen)]$ (**1**) was found and thermal-induced as well as

light-induced spin-state switching of a submonolayer of **1** was detected.[32] This raises the question of whether the decomposition of this complex observed on Au(111) can also be suppressed by deposition on, e.g., bismuth. Possibly this substrate would also enable thermal- or light-induced spin crossover in mono- or submonolayers, which so far has not been achieved for monolayers of **1** and the related complex [Fe(H$_2$B(pz)$_2$)$_2$(bipy)] on Au(111).[33] In fact, the lack of switching of molecules deposited on Au(111) has in some cases been remedied by deposition on Bi(111) or Bi(110).[34] Bismuth is a semimetal with a low density of states at the Fermi level, thus reducing van der Waals interactions with aromatic substrates in direct contact with the surface.[35] With regard to the complex [Fe(H$_2$B(pz)$_2$)$_2$(phen)] (**1**), this could also reduce the interaction between phenanthroline and the solid surface and thus prevent the decomposition of **1**.

A second possible strategy of reducing the interaction between complex **1** and a solid surface is the attachment of substituents to the ligand 1,10-phenanthroline. [Fe(H$_2$B-(pz)$_2$)$_2$(L)] complexes with methylated 1,10-phenanthroline,[36,37] annulated 2,2′-bipyridine,[38] diarylethene,[39−41] or π-radical ligands[42] have been reported. In order to evaluate this approach in the present context, we have prepared the new spin-crossover complex [Fe(H$_2$B(pz)$_2$)$_2$(phenme$_4$)] (**2**) (Figure 1), in which phen is replaced by 3,4,7,8-tetramethyl-1,10-
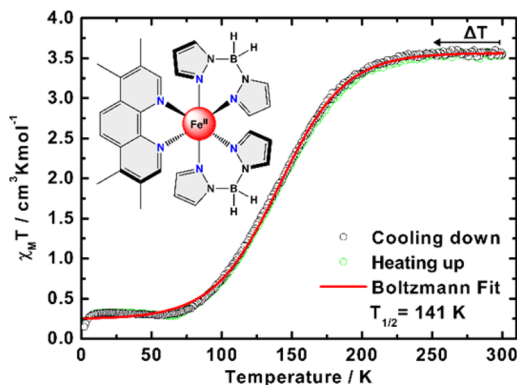
Figure 1. $\chi_M T$ vs T curves of crystalline **2** between 2 and 300 K. The curves resulting from cooling (black symbols) and heating (green symbols) the sample almost coincide. The temperature-induced SCO is fitted by a Boltzmann equation (red line) to obtain $T_{1/2}$. Inset: molecular structure of **2**.

phenanthroline (phenme$_4$). Herein, the spin-crossover behavior of **2** is first determined in the bulk by temperature-dependent susceptibility measurements and Mößbauer spectroscopy. Moreover, thin films of **2** are prepared by physical vapor deposition on glass and studied by optical absorption spectroscopy. Finally, submonolayers of **2** are deposited on the two substrates, Au(111) and Bi(111), and studied by temperature-dependent near-edge X-ray absorption fine structure (NEXAFS) as well as low-temperature STM. The results are compared to similar data obtained with the parent compound **1** deposited on Au(111) and Bi(111) and provide insight into the structural and electronic properties of submonolayers of this class of SCO complexes in direct contact with solid surfaces.

■ RESULTS AND DISCUSSION

The synthesis and the physicochemical properties of the complex [Fe(H$_2$B(pz)$_2$)$_2$(phen)] (**1**) in the bulk as well as in thin films deposited on Au(111) and HOPG have been reported before.[9,14,17,19−21,23,31,32] In analogy to the synthesis of **1**, a microcrystalline powder of [Fe(H$_2$B(pz)$_2$)$_2$(phenme$_4$)] (**2**) was obtained with methanol as solvent, starting from iron(II) triflate as precursor.[17,36] To analyze the thermal spin crossover of **2** in the solid state, magnetic susceptibility measurements were performed (Figure 1).

The new complex shows a gradual spin transition with $\chi_M T$ values ranging from 3.56 cm^3 K mol^{-1} at 300 K to 0.27 cm^3 K mol^{-1} at 5 K; the spin transition temperature $T_{1/2}$ is 141 K. This behavior is similar to other analogues of **1**.[36]

To obtain further information on the spin state of the iron center, Mößbauer spectra were recorded at 298 and 80 K (Figure 2). At 298 K compound **2** shows a doublet with δ_{HS} =
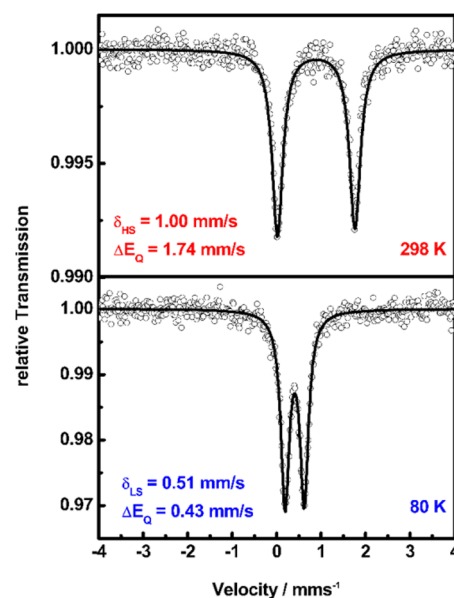
Figure 2. Mößbauer spectra of **2** at 298 (top) and 80 K (bottom).

1.00 mm/s and ΔE_Q = 1.74 mm/s, indicative of high-spin iron(II) centers.[6,36] At 80 K one doublet at δ = 0.51 mm/s and ΔE_Q = 0.43 mm/s is observed, indicating a low-spin iron(II) species.[6,36] Mößbauer spectra were also recorded at 141 and 151 K to determine the HS/LS ratio around the spin transition temperature; the results agree with the magnetic susceptibility measurements (see Supporting Information, Figures S1 and S2).

Compound **2** can be evaporated at T = 175 °C, p = 3 × 10^{-2} mbar, or at 163 °C in an ultrahigh vacuum (∼10^{-8} Pa). Differential thermoanalysis along with thermogravimetry (DTA/TG) shows that complex **2** is stable up to about 200 °C, where decomposition starts to take place (see Supporting Information, Figure S3). The structural integrity of the complex in the vacuum-deposited films is, e.g., evident from the fact that infrared spectra of the film are found to be very similar to those recorded from microcrystalline material.[36] In particular, the symmetric and antisymmetric B−H vibrations are detected both in the bulk material and in the film at ν_{asym}(B−H) = 2389 cm^{-1} and ν_{sym}(B−H) = 2285 cm^{-1}, which indicates the integrity of the coordination sphere (Figure 3). Furthermore, elemental analysis of evaporated material shows no major
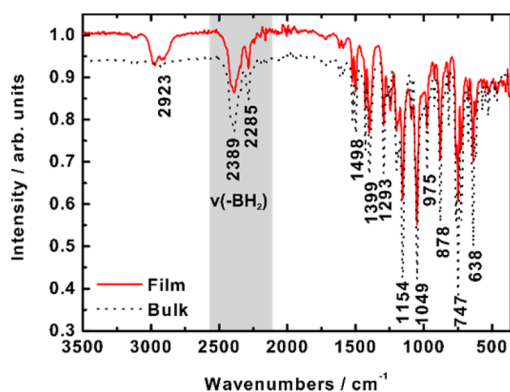
Figure 3. Fourier transform infrared (FT-IR) spectra of bulk material (black dotted line) and vacuum-deposited material (red line) of **2** at 298 K.

changes compared to the bulk material, and, most importantly, the thermal spin-crossover properties of the complex are retained.

For a film of compound **2**, the metal-to-ligand charge transfer (MLCT) bands at 298 K evolve to a more intense double-band pattern centered at 539 and 600 nm at 78 K (Figure 4).
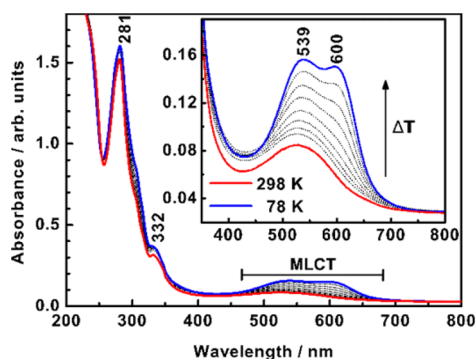
Figure 4. Temperature-dependent UV/vis spectra of a vacuum-deposited film of compound **2** on a quartz disk at 298 (red line) and 78 K (blue line). Gray: intermediate temperatures.

Similar observations have been made for analogous complexes, indicating thermal spin crossover from HS to LS.[21,36] Moreover, the vacuum-deposited film of **2** exhibits the *light-induced excited spin-state trapping* (LIESST) effect;[43,44] i.e.,

at 5 K the low-spin state can be converted back to the high-spin state by irradiation at 519 nm for 5 min (Figure 5a). In Figure 5b, the high-spin fraction γ_{HS} derived from the intensity of the MLCT band is displayed versus the temperature.[21,36] The thermal transition is more gradual than in the bulk (cf. Figure 1), presumably due to weaker cooperative interactions in the vacuum-deposited film. The thermal spin transition temperature $T_{1/2}$ is 148 K, slightly higher than in the bulk (see above), and the critical temperature for the HS-to-LS relaxation is $T_c = 54$ K.

XA Spectroscopy in Submonolayers. In order to investigate the physicochemical properties of the new complex **2** in direct contact with a solid surface, it was deposited on Bi(111) and Au(111) with coverages of 0.3 and 0.6 ML, respectively (ML = monolayer). The results are compared to 0.3 ML of the parent complex **1** on Bi(111). To probe the spin states, Fe L_3 edge XA spectra (Figure 6a,b) were recorded at the magic angle between the substrate normal and the electric field vector of the X-rays (at the magic angle, 54.7°, the X-ray absorption is independent of the polarization direction of the beam). On Bi(111), the room-temperature XA spectra at the Fe L_3 edge exhibit two main peaks at 708.1 and 708.8 eV and two broad satellite peaks centered at ∼706.5 and ∼710.9 eV, as shown in Figure 6a (red line). The spectral shape changes gradually as the temperature is decreased to 60 K, marked by a gradual decrease of the peak intensity at 708.1 eV, the emergence and subsequent intensity increase of a peak at 709.3 eV, and a slight energy shift (accompanied by a relative intensity increase) of the satellite peak from ∼710.9 to ∼711.5 eV. This is characteristic of SCO complexes undergoing a thermal spin transition.[13,45] The observed Fe L_3 spectral shape at room temperature (RT) indicates a dominant HS state, and the emergence and gradual intensity increase of the peak at 709.3 eV with decreasing temperature reflect the conversion of the HS to the LS state. Details of the decomposition into HS and LS spectral components are shown in the Supporting Information. Upon further lowering the temperature from 60 K at a rate of 4 K/min, however, the LS species gradually switches back to the HS species, increasing with each successive measurement. This is due to soft X-ray induced excited spin state trapping (SOXIESST).[46] Similar Fe L_3 XA edge spectra are observed for 0.3 ML of the parent complex **1** on the same Bi(111) surface (Figure 6c). The spectrum at 300 K exhibits the characteristic HS shape with the main peaks at 708.1 and 708.8 eV. Upon lowering the temperature, the intensity of the
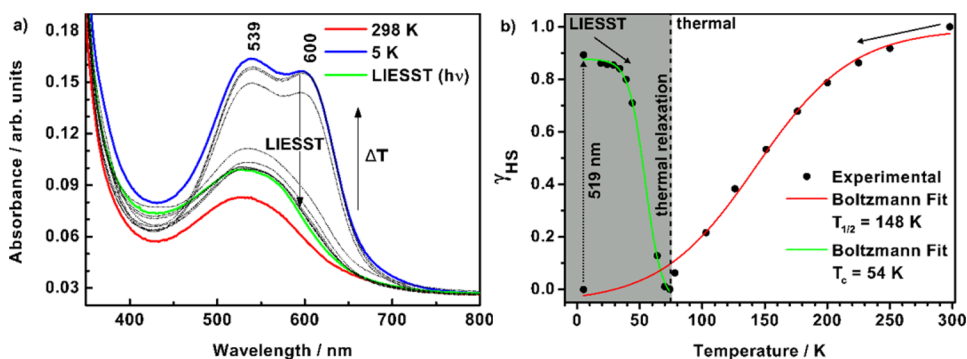
Figure 5. (a) Temperature-dependent UV/vis spectra of a vacuum-deposited film of compound **2** on a quartz disk at 298 (red line) and 5 K (blue line), and LIESST at 5 K (green line). Gray traces show spectra taken during thermal relaxation of the LIESST state. (b) High-spin fraction γ_{HS} vs T along with Boltzmann fit (red line). The light-induced SCO at 5 K is shown by a dotted black arrow, and the thermal HS-to-LS relaxation is shown by a Boltzmann fit (green line).
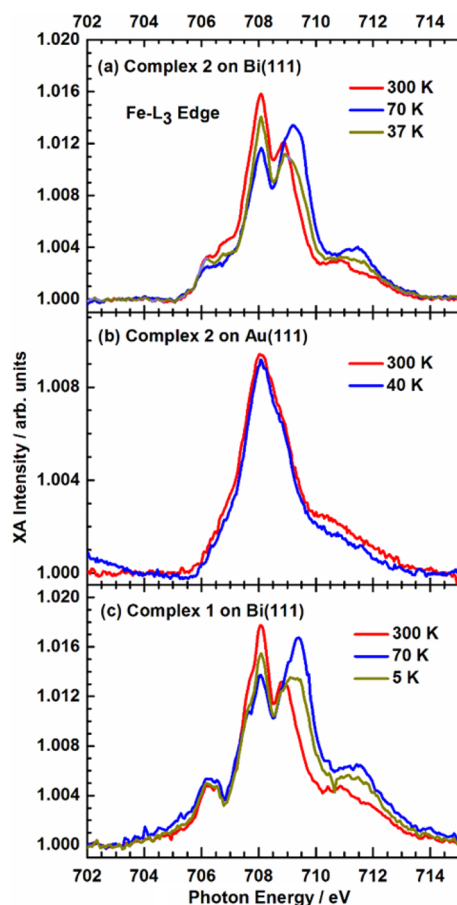
Figure 6. (a) Fe L$_3$ edge XA spectra of 0.3 ML of **2** on Bi(111) at 300 K (red line), at 70 K (blue line), and at 37 K (olive line), indicating the SCO behavior, and (b) Fe L$_3$ edge XA spectra of 0.6 ML of **2** on Au(111) at 300 K (red line) and at 40 K (blue line), indicating the loss of SCO behavior. (c) Fe L$_3$ edge XA spectra of 0.3 ML of **1** on Bi(111) at 300 K (red line), at 70 K (blue line), and at 5 K (olive line), indicating the SCO behavior. All spectra are recorded at the magic angle.

HS peaks is reduced and the intensity of the peak at 709.3 eV characteristic of the LS state increases. At 5 K, X-ray induced back switching from LS to HS occurs.

For 0.6 ML of **2** on Au(111), in contrast, the Fe L$_3$ edge XA spectrum exhibits no such change in the spectral shape with temperature. Figure 6b shows the Fe L$_3$ edge XA spectra at 300 K (red line) and at 40 K (blue line). Here, the spectra are

characterized from 300 K down to low temperature by a single peak at 708.1 eV without an apparent multiplet structure. This is an indication of the loss of SCO behavior, possibly due to fragmentation of the molecule. In fact, N K edge XA spectra and STM measurements show that [Fe(H$_2$B(pz)$_2$)$_2$(phenme$_4$)] (**2**) dissociates into phenme$_4$ and the tetrahedral complex [Fe(H$_2$B(pz)$_2$)$_2$] (see below). Similar results had been obtained earlier for 0.8 ML of complex **1** deposited on Au(111): the Fe L$_3$ edge XA spectrum is characterized by a single peak at 708.1 eV with no apparent multiplet structure, and the spectral shape is independent of temperature from 300 K down to 5 K.[31] The loss of SCO behavior has been confirmed as being due to the dissociation of **1** into [Fe(H$_2$B(pz)$_2$)$_2$] and phen on Au(111), with SQUID, XAS, and STM measurements.[31] The SQUID measurement of bulk material of [Fe(H$_2$B(pz)$_2$)$_2$] shows that it is in HS state from 300 K down to 25 K, in agreement with its tetrahedral geometry.[47] For 1.3 ML of [Fe(H$_2$B(pz)$_2$)$_2$] on Au(111), the Fe L$_3$ edge XA spectrum consists of a single peak at 708.1 eV at 300 K,[31] similar to that of 0.6 ML of **2** on Au(111), while the distinguishing feature between 0.6 ML of **2** and 1.3 ML of [Fe(H$_2$B(pz)$_2$)$_2$] on Au(111) in the N K edge XA spectrum can be seen in the presence or absence of the π^* resonance at 399.1 eV, respectively.

It can thus be concluded that the functionalization of the phenanthroline ligand with four methyl groups does not help to preserve the integrity of the complex on Au(111). On the other hand, both complexes **1** and **2** remain intact on Bi(111), as also indicated by the angle-dependent N K edge XA data (see below). Moreover, both exhibit qualitatively similar thermal SCO behavior, as can be inferred from the temperature-dependent Fe L$_3$ edge XA spectral shape (Figure 6a,c).

More quantitative information on this issue is obtained from a determination of the high-spin fraction γ_{HS} as a function of temperature. Owing to the similar temperature-dependent Fe L$_3$ edge XA spectra of **1** and **2**, and the data of **1** on HOPG,[32] the latter can be used as a reference for the pure HS and LS spectra (**1** exhibits 91(5)% HS at 300 K and 100% LS at 6 K on this substrate). To determine the high-spin fractions γ_{HS} of **1** and **2** on Bi(111) at different temperatures, these reference spectra are linearly combined (see Supporting Information). For the parent complex **1** on Bi(111) (Figure 7a, red dots), the HS fraction at 300 K is estimated as 88(5)%, decreasing to 46(5)% at 71 K. At lower temperatures, the HS fraction increases gradually due to the SOXIESST effect, rising to about 60(5)% HS at 5 K (cf. Figure 6c, olive line). The increase in the
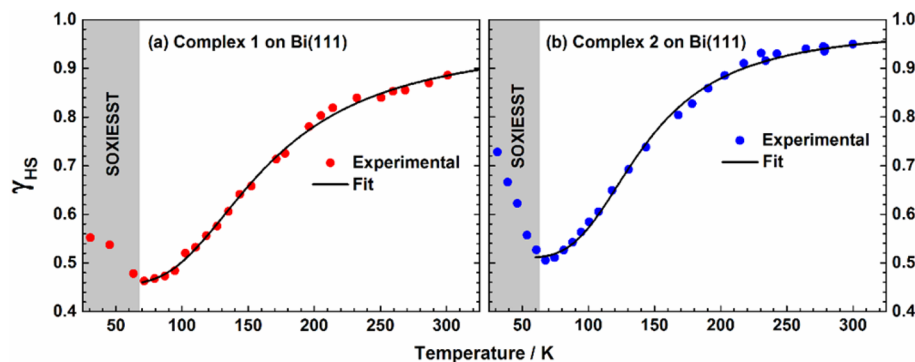
Figure 7. Temperature dependence of the high-spin fraction γ_{HS} of (a) 0.3 ML of **1** on Bi(111) (red dots) and (b) 0.3 ML of **2** on Bi(111) (blue dots). The black lines are the fits obtained from the van't Hoff equation [eq 1].
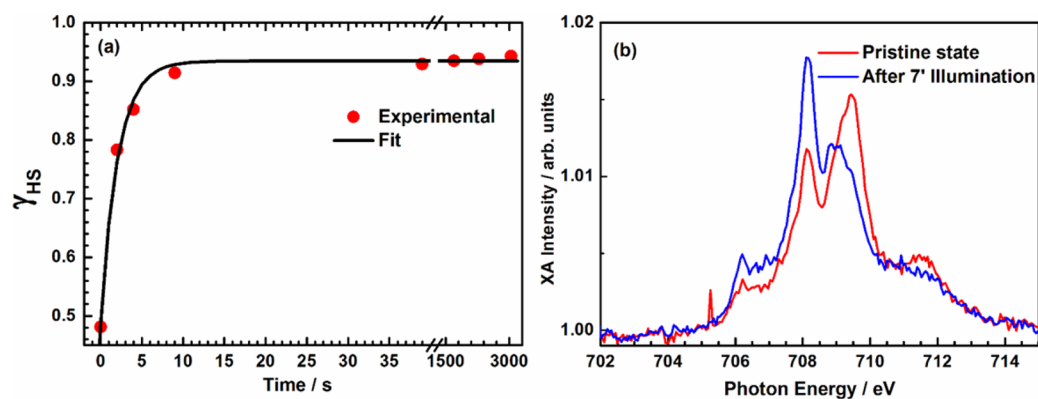
Figure 8. Light-induced (LIESST) switching of (a) 0.3 ML of **2** on Bi (111) at 17 K and (b) 0.3 ML of **1** on Bi(111) at 5 K: Fe L_3 edge XA spectrum before illumination (red line) and after 7 min of illumination (blue line).

HS fraction with increasing exposure time of the sample to the X-ray beam is in part due to the fact that the XA spectra are measured successively at the same spot during the cooling process. For complex **2**, on the other hand, the HS fraction at 300 K is estimated as 95(5)%, decreasing to 51(5)% at 68 K before the onset of SOXIESST (Figure 7b, blue dots).

The temperature dependence of the high-spin fractions (γ_{HS}) of **1** and **2** can be described with a modified van't Hoff equation, taking the partial nature of the spin switching process into account:

$$\gamma_{HS}(T) = a + (1 - a)(e^{\Delta H/RT - \Delta S/R} + 1)^{-1} \quad (1)$$

Here, constant a corresponds to the fraction of molecules trapped in the HS state at all temperatures, ΔH and ΔS are enthalpy and entropy differences between HS and LS states, respectively, and R is the universal gas constant. From the fit of the experimental data between 300 and 70(60) K, respectively, ΔH is estimated as 4.6(1) and 5.1(1) kJ mol^{-1}, and ΔS as 26.3(6) and 34.6(8) J K^{-1} mol^{-1}, for **1** and **2**, respectively. The temperature-independent high-spin fraction a amounts to 46(5)% for **1** and 51(5)% for **2**.

Complex **2** exhibits pronounced X-ray and light-induced spin-state switching from the LS to the HS state, as shown for LIESST in Figure 8a (see Figure S2 of the Supporting Information for SOXIESST). Illumination at 17 K for <1 min with a wavelength of 520 nm under a photon flux of 2.5(5) × 10^{17} photons/s/cm^2 increases the high-spin fraction of complex **2** from 48(5) to 94(5)%; upon further illumination the population remains constant. From an exponential fit, the time constant for the light-induced switching process under these conditions is estimated as 2.1(1) s. It should be noted that the spectra were recorded on a virgin position of the sample that had not been exposed to X-rays before in order to start with minimum SOXIESST. There is, however, a contribution to the switching process by X-rays, as is shown in the Supporting Information.

Although no time-dependent measurements have been performed for **1** under illumination, clear evidence for the LIESST effect is obtained for this molecule deposited on Bi(111) as well. Figure 8b shows XA spectra at the Fe L_3 edge for the pristine sample at 5 K (red line) and after 7 min illumination (blue line) with a wavelength of 520 nm under a photon flux of 4.0(8) × 10^{16} photons/s/cm^2. At 5 K in the pristine state, γ_{HS} is determined as 48(5)%; after 7 min illumination, it increases to 80(5)%.

To obtain information on the adsorption geometries of **1** and **2** on Bi(111) and Au(111) and to estimate molecular orientations of these molecules and their possible decomposition products on the two surfaces, angle-dependent XA spectra at the N K edge were measured at 300 K. Three incidence angles between the electric field vector of the X-rays and the surface normal were employed, i.e., θ = 90°, 54.7° (magic angle), and 25°. The resulting spectra are presented in Figure 9, parts a and b, for complex **2** on Au(111) and Bi(111), respectively, and in Figure 9c for complex **1** on Bi(111). The
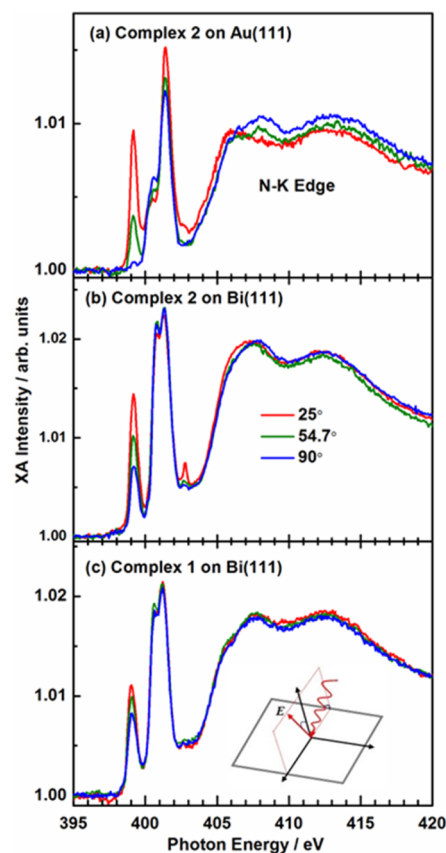
Figure 9. (a) N K edge XA spectra of 0.6 ML of **2** on Au(111), (b) N K edge XA spectra of 0.3 ML of **2** on Bi(111), and (c) N K edge XA spectra of 0.3 ML of **1** on Bi(111) taken at grazing (25°), magic (54.7°), and normal (90°) angles between the surface normal and the electric field vector of the incoming X-ray beam at 300 K.
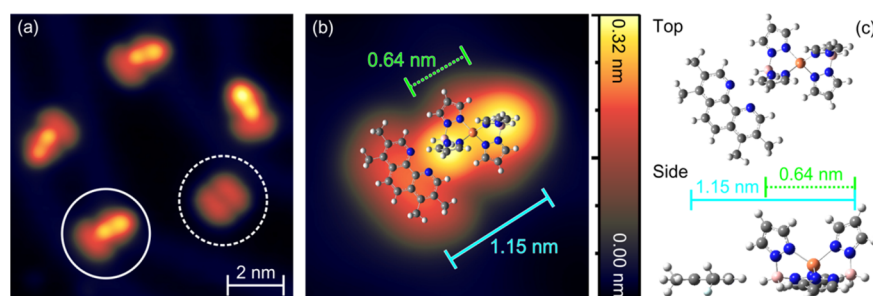
Figure 10. (a, b) Constant-current topographs of $[Fe(H_2B(pz)_2)_2(phenme_4)]$ **2** prepared on Au(111) at ambient temperature. The overview image in (a) shows two typical patterns. The first pattern (example marked by solid circle) consists of two high protrusions and a shallow bean-shaped elevation at one end. It is attributed to tetrahedral $[Fe(H_2B(pz)_2)_2]$ adjacent to a single phenme$_4$. The second pattern (dashed circle) is comprised of two symmetrically arranged bean-shaped features. By analogy with earlier observations,[31] we identify it as being due to phenme$_4$ dimers. (c) Top and side views of the calculated structure of $[Fe(H_2B(pz)_2)_2]$ and phenme$_4$ interacting in the gas phase. Two characteristic dimensions are indicated. The calculated structure is superimposed onto the STM image in (b).

π^* resonance at 399.2 eV stems from the two N atoms of the phenme$_4$ ligand, and the shoulder at 400.6 eV and the peak at 401.4 eV are π^* resonances from N atoms of the $H_2B(pz)_2$ ligands.[31] From the XA intensity ratio between spectra taken at 25 and 90° incidence angles, the molecular orientation of the respective orbitals on the surface can be determined.[48] Accordingly, the phenme$_4$ ligands are found to lie flat on the Au(111) surface for complex **2** on Au(111) (Figure 9a), indicating a disintegration of this complex. From the peak intensity at 401.4 eV, the delocalized orbitals of the $H_2B(pz)_2$ ligands are estimated to lie at $\sim$51(5)° with respect to the substrate normal, which is close to the magic angle of 54.7°. This could also be due to a random orientation of the pyrazole units of the two $H_2B(pz)_2$ ligands on the surface.

These findings, including the spectral shape of both the N K edge and Fe L$_3$ edge spectra, are similar to the results of previous studies obtained on 0.8 ML of complex **1** on Au(111).[31] Thus, it can be concluded from XA spectroscopy that the addition of four methyl groups to the ligand 1,10-phenanthroline does not prevent fragmentation of **2** to phenme$_4$ and $[Fe(H_2B(pz)_2)_2]$ on the Au(111) surface; i.e., **2** behaves just like the parent molecule **1** on this substrate.

For complex **2** on Bi(111), in contrast, the delocalized π^* orbitals from the $H_2B(pz)_2$ ligands with peaks at 400.6 and 401.4 eV show nearly no angle dependence of the intensity (Figure 9b), which indicates that the $H_2B(pz)_2$ ligands either lie at the magic angle with respect to the Bi(111) surface or are randomly oriented on the surface. On the other hand, the plane of the phenme$_4$ ligand lies 44(5)° away from the surface. Since after breaking of the molecule into $[Fe(H_2B(pz)_2)_2]$ and phenme$_4$ the latter is expected to be adsorbed flat on the surface (see above), this is an indication of the integrity of $[Fe(H_2B(pz)_2)_2](phenme_4)]$ (**2**) on Bi(111) which may be ascribed to the weaker interaction between **2** and this surface as compared to Au(111).[31] Similar results can be inferred from the angle-dependent XA spectra of **1** deposited on Bi(111) (Figure 9c). Here the angle of the phen ligand to the surface is 49(5)°, which indicates that complex **1** is intact on this surface as well.

STM Measurements in Submonolayers. For a microscopic investigation of the new complex $[Fe(H_2B(pz)_2)_2(phenme_4)]$ (**2**) on Au(111), STM measurements were performed under ultrahigh vacuum conditions at 4.5 K. Figure 10a displays a typical constant-current image of a surface prepared at ambient temperature. We observe two classes of objects. First, there is a pattern of two protrusions (0.305 $\pm$

0.01 nm apparent height) along with a more shallow bean-shaped elevation at one end. Second, we observe a symmetric pattern that is comprised of two bean-shaped features. The latter pattern appears familiar from earlier results from compound **1** on Au(111), where it was shown to be due to two 1,10-phenanthroline (phen) molecules arranged into a dimer.[31] Thus, we identify the symmetric pattern found here as a dimer of two phenme$_4$ molecules. Phenme$_4$ appears approximately 0.4 nm longer than phen, which is consistent with the presence of its four methyl groups. The former structure is shown in more detail in Figure 10b. We attribute it to a single phenme$_4$ molecule adjacent to tetrahedral $[Fe(H_2B(pz)_2)_2]$ (see XA Spectroscopy in Submonolayers). In our model, the two topographic maxima correspond to protruding pyrazole groups of $[Fe(H_2B(pz)_2)_2]$. The drastic height difference between the upper part of these groups and the rest of the molecule (calculated value by density functional theory (DFT), 0.38 nm) is expected to largely dominate the image contrast. Therefore, a geometric interpretation of the STM topograph is a useful approximation.

The gas-phase structures of the single $[Fe(H_2B(pz)_2)_2]$ and phenme$_4$ molecules as calculated with DFT are shown in Figure 10c. They are arranged to a bimolecular cluster which is overlaid onto the STM image in Figure 10b. We find good agreement of the separation between the maxima in the STM topograph of 0.63 $\pm$ 0.02 nm and the calculated distance of the pyrazole groups of 0.64 nm. To further test the model, we performed DREIDING force-field calculations that mimic the interaction between the $[Fe(H_2B(pz)_2)_2]$ and phenme$_4$ molecules in the gas phase (Figure 10b,c). The calculated distance between phenme$_4$ and the more remote $[Fe(H_2B(pz)_2)_2]$ group is 1.15 nm. It is consistent with the measured STM data of 1.17 $\pm$ 0.06 nm. According to the calculations, the observed arrangement of $[Fe(H_2B(pz)_2)_2]$ and phenme$_4$ is stabilized by several hydrogen bonds, namely three B–H $\rightarrow$ N(phen) and two C(pyrazole)–H $\rightarrow$ N bonds. This may explain the experimental observation that most of the $[Fe(H_2B(pz)_2)_2]$ and phenme$_4$ molecules arrange into bimolecular clusters with a specific geometry on Au(111). The separation of phenme$_4$ and the iron center of $[Fe(H_2B(pz)_2)_2]$ ($\sim$0.86 nm) is significantly larger than expected for a coordinative bond. In fact, we did not observe structures that indicate the presence of the undistorted compound **2**.

Breaking of a coordinative bond by adsorption to gold may appear unusual. However, the STM data clearly show that $[Fe(H_2B(pz)_2)_2(phenme_4)]$ (**2**) dissociates into $[Fe(H_2B-

$(pz)_2)_2]$ and phenme$_4$ on Au(111) at ambient temperature. We assume that **2** is destabilized by dispersion interactions between the molecule and the substrate. Similar results are obtained for compound **1** on Au(111). For low coverage, the fragments of **1** form similar bimolecular clusters as the fragments of complex **2** (see Supporting Information, Figure S6). In ref 31, we showed an image which demonstrates the decomposition of **1** on Au(111) for higher coverage. Recent theoretical work indeed shows that dispersion interactions can influence the relative stability of molecules on metal surfaces.[49]

We made various attempts to switch the molecules of **2** adsorbed to Au(111) in the STM, both by injecting electrons or holes at elevated energies and currents and by pushing molecules with the tip, but did not observe any indication of a spin transition. This negative result agrees with the observations from XA spectroscopy.

■ CONCLUSIONS

The complex $[Fe(H_2B(pz)_2)_2(phen)]$ (**1**) is known to decay on Au(111) into the four-coordinate complex $[Fe(H_2B(pz)_2)_2]$ and phen. To suppress this reaction, two approaches have been pursued in the present paper. The first one aims at reducing the molecule−substrate interaction by introducing a ligand which presumably is less weakly bound to the metal surface. The second approach involves using Bi(111) as a substrate because Bi is known to lower the strength of the dispersion interaction with aromatic molecules relative to gold. The new complex **2** is found to be suitable for vacuum deposition to obtain molecular layers. Combined evidence from NEXAFS and STM, however, indicates that in a submonolayer deposited on Au(111) at room temperature this molecule dissociates into a four-coordinate complex, $[Fe(H_2B(pz)_2)_2]$, and phenme$_4$. This finding is similar to the result of previous studies of the parent molecule $[Fe(H_2B(pz)_2)_2(phen)]$ (**1**).[31] Apparently the introduction of four methyl groups cannot suppress the decay of this type of SCO complexes on Au(111). In contrast, temperature-dependent NEXAFS measurements of a submonolayer of **2** deposited on Bi(111) indicate thermal-, light-, and X-ray-induced spin-state switching processes. Specifically, we find light-induced spin-state switching at 17 K. Below 60 K, excitation to the high-spin state is further mediated by the SOXIESST effect, which is in agreement with other examples reported.

Similar results are obtained for the parent complex $[Fe(H_2B(pz)_2)_2(phen)]$ (**1**) deposited on Bi(111). These observations thus indicate that complexes **1** and **2** stay intact on Bi(111), rendering this substrate a useful alternative to Au(111) in cases where the strong van der Waals interactions mediated by the Au(111) surface lead to a disintegration of functional molecules. In contrast to the behavior of **1** on HOPG, however, where γ_{HS} can be switched between 0 and almost 100%,[32] only about half of the molecules of **1** and **2** on Bi(111) undergo a spin transition whereas the others remain in the HS state. The suppression of the spin transition for the latter may be ascribed to differences in the adsorption geometry leading to a variation in the interaction with the Bi(111) surface. Alternatively, the differences in SCO behavior could be due to lateral interactions between the molecules in the two-dimensional layer which may mediate elastic forces similar to the behavior of SCO complexes observed in some bulk materials.[50] In fact, a mixture of HS and LS molecules was found for a submonolayer of $[Fe((3,5-(CH_3)_2pz)_3BH)_2]$ on Au(111) in which at 4.6 K HS and LS molecules are both present and form an ordered superstructure.[15] Since we do not

have any information about the morphology on Bi(111), we also cannot exclude the possibility that the molecules form clusters or multilayer islands, and that the nonswitching fraction is the molecules that are in direct contact with the surface. Understanding the exact conditions for spin-state switching of transition-metal complexes on solid surfaces and elucidating possible factors that influence or limit the switchability of these molecules on surfaces thus remain challenging problems in the area of spintronics.

■ EXPERIMENTAL SECTION

All reactions were carried out in dry solvents and under inert atmosphere. Functionalized 3,4,7,8-tetramethyl-1,10-phenanthroline, iron(II) triflate, and solvents were purchased commercially and used as supplied. Potassium dihydrobis-(pyrazolyl)borate $K[H_2B(pz)_2]$ and complex **1** were prepared according to literature methods.[17,51]

Synthesis of $[Fe(H_2B(pz)_2)_2(3,4,7,8$-tetramethyl-1,10-phenanthroline)]$ (2). To a solution of Fe(OTf)$_2$ (354 mg, 1 mmol) in methanol (5 mL) was added a solution of $K(H_2B(pz)_2)$ (372 mg, 2 mmol) in methanol (5 mL); a slightly yellow solution was obtained. A solution of 3,4,7,8-tetramethyl-1,10-phenanthroline (236 mg, 1 mmol) in methanol (10 mL) was added dropwise to the $[Fe(H_2B(pz)_2)_2]$ solution. Immediately, a purple precipitate was formed, filtered off after 1 h, washed with methanol (2 × 5 mL), and dried under reduced pressure. Yield: 429 mg (0.73 mmol, 73%). Elemental analysis calculated for **2**: C, 57.38%; H, 5.54%; N, 23.90%; found: C, 57.19%; H, 5.49%; N 23.87%. Elemental analysis after physical vapor deposition (T = 175 °C, p = 3 × 10^{-2} mbar) calculated for **2**: C, 57.38%; H, 5.54%; N, 23.90%; found: C, 57.17%; H, 5.86%; N, 23.89%.

XA Spectroscopy. The samples, i.e., 0.3 ML of **1** and **2** on Bi(111) and 0.6 ML of **2** on Au(111), were prepared by evaporating the molecular powder from a tantalum Knudsen cell at about 436 K onto the substrate held at RT. The evaporation rate and hence the amount of molecules deposited on the surface were monitored by a quartz microbalance. The molecular coverage was further estimated from the absolute Fe L$_3$ edge resonance intensity, using the procedure described elsewhere.[31] One monolayer is defined as having an areal density of 0.82 Fe ion/nm^2, the same as in ref 31. The substrates were cleaned by the standard procedure of repeated sputtering with Ar$^+$ ions, followed by annealing at 900 K for Au(111) and 300 K for Bi(111) substrates. The XAS measurements were carried out in situ at a base pressure of 5 × 10^{-10} mbar at the beamline UE56/2-PGM-2 for complex **2**, and for complex **1** at the beamline UE46-PGM1 of BESSY II with a base pressure of 5 × 10^{-11} mbar. The photon flux at the sample position was ≈10^{13} photons s^{-1} cm^{-2} with the energy resolution at ≈200 meV for the former, and the photon flux of ≈10^{11} photons s^{-1} cm^{-2} and the energy resolution at ≈150 meV for the latter beamline. To probe the thermal SCO behavior and the stability of the molecule, Fe L$_3$ edge and N K edge XA spectra were recorded at the magic angle of 54.7° as well as at 25 and 90° between the surface normal and the electric field vector of the linearly polarized X-rays. The spectra at 25 and 90° were used for the determination of the molecular orientation. The mode of illuminations used to induce the LIESST effect has been described elsewhere.[31] XA was measured by the total electron yield mode, where the sample drain current is recorded as a function of photon energy. The XA spectra were normalized with respect to a gold grid

upstream to the experiment and to the background signal from clean Au(111) and Bi(111) substrates.

Scanning Tunneling Measurements. STM measurements were performed with a homemade STM operated at 4.5 K and in ultrahigh vacuum with a base pressure of 10^{-9} Pa. Au(111) surfaces and chemically etched W tips were cleaned by repeated Ar^+ bombardment and annealing. The apexes of the tips were covered with Au by repeatedly indenting the tip into the Au(111) surface. $[Fe(H_2B(pz)_2)_2(phenme_4)]$ molecules were deposited onto Au(111) at ambient temperature from a heated Ta crucible. The pressure during depositions was 10^{-8} Pa. To get submonolayer coverages, the deposition rate was calibrated with the help of a quartz balance and the deposition time was adjusted. The submonolayer coverages were verified by STM images. All images were acquired in the constant-current mode of the STM with the voltage applied to the sample.

DFT and DREIDING Force Field Calculations. DFT calculations were performed for isolated $phenme_4$ with B3LYP[52−54]/6-311G[55−62] and for $[Fe(H_2B(pz)_2)_2]$ with TPSSH[63]/TZVP[64,65] as implemented in the Gaussian 09 software package.[66] DREIDING force-field calculations were performed to model the interaction between $phenme_4$ and $[Fe(H_2B(pz)_2)_2]$ in the gas phase.[67] The DFT geometry of $[Fe(H_2B(pz)_2)_2]$ was kept frozen during the force-field relaxation, because the structure of $[Fe(H_2B(pz)_2)_2]$ is not well described by the DREIDING force fields due to the spin state of the molecule. Furthermore, to model the influence of the surface in the gas phase calculations, the orientation of $phenme_4$ relative to $[Fe(H_2B(pz)_2)_2]$ was confined parallel to the plane shown in the top view of Figure 10c.

Other Measurements. Elemental analyses were performed using a Euro Vector CHNS-O-element analyzer (Euro EA 3000). Samples were burned in sealed tin containers by a stream of oxygen. IR spectra were recorded on a Bruker Alpha-P ATR-IR spectrometer. Magnetic measurements were performed with a temperature circle from 300 K to 2 K to 300 K using a physical property measurement system (PPMS, Quantum Design) and a magnetic field strength of 1 T. Diamagnetic corrections were applied with the use of tabulated Pascal's constants. Mößbauer measurements were recorded with a self-assembled spectrometer using standard transmission geometry. UV/vis spectra were recorded with a Cary 5000 spectrometer in transmission geometry. For temperature dependence, a CryoVac cryostat with liquid nitrogen or helium cooling was used. The compound was evaporated as films on quartz disks at T = 175 °C, p = 3 × 10^{-2} mbar (thickness several 100 nm), under the same conditions as in refs 21 and 36. For illumination experiments, a 3× LED Luxeon Typ LXML-PM01-0080 (λ = 519 nm) from Sahlmann Photochemical Solutions was used.

ASSOCIATED CONTENT

ⓢ Supporting Information

The Supporting Information is available free of charge on the ACS Publications website at DOI: 10.1021/acs.jpcc.6b10888.

Mößbauer spectra around the spin transition temperature compared to magnetic susceptibility measurements, DTA/TG measurements of **2**, Fe L_3 absorption spectra of 0.4 ML of $[Fe(H_2B(pz)_2)_2(phen)]$ (**1**) on HOPG, Fe L_3 absorption spectra of 0.3 ML of $[Fe(H_2B-(pz)_2)_2(phenme_4)]$ (**2**) on Bi(111) at 300 K and at 70 K, X-ray-induced spin-state switching plot of **1** on Bi(111) at 5 K, and that of **2** on Bi(111) at 17 K, STM image of **1** for low coverage (PDF)

AUTHOR INFORMATION

Corresponding Authors
*E-mail: kuch@physik.fu-berlin.de.
*E-mail: berndt@physik.uni-kiel.de.
*E-mail: ftuczek@ac.uni-kiel.de.

ORCID 🄭

Felix Tuczek: 0000-0001-7290-9553

Notes

The authors declare no competing financial interest.

REFERENCES

(1) Kahn, O.; Martinez, C. J. Spin-Transition Polymers: From Molecular Materials Toward Memory Devices. *Science* **1998**, *279*, 44−48.

(2) Halcrow, M. A. *Spin-Crossover Materials*, 1st ed.; Wiley: Chichester, U.K., 2013.

(3) Hayami, S.; Holmes, S. M.; Halcrow, M. A. Spin-State Switches in Molecular Materials Chemistry. *J. Mater. Chem. C* **2015**, *3*, 7775−7778.

(4) Gütlich, P. Spin Crossover − Quo Vadis? *Eur. J. Inorg. Chem.* **2013**, *2013*, 581−591.

(5) Molnár, G.; Salmon, L.; Nicolazzi, W.; Terki, F.; Bousseksou, A. Emerging Properties and Applications of Spin Crossover Nanomaterials. *J. Mater. Chem. C* **2014**, *2*, 1360−1366.

(6) Gütlich, P.; Gaspar, A. B.; Garcia, Y. Spin State Switching in Iron Coordination Compounds. *Beilstein J. Org. Chem.* **2013**, *9*, 342−391.

(7) Auwärter, W.; Écija, D.; Klappenberger, F.; Barth, J. V. Porphyrins at Interfaces. *Nat. Chem.* **2015**, *7*, 105−120.

(8) Miyamachi, T.; Gruber, M.; Davesne, V.; Bowen, M.; Boukari, S.; Joly, L.; Scheurer, F.; Rogez, G.; Yamada, T. K.; Ohresser, P.; et al. Robust Spin Crossover and Memristance across a Single Molecule. *Nat. Commun.* **2012**, *3*, 938.

(9) Gopakumar, T. G.; Matino, F.; Naggert, H.; Bannwarth, A.; Tuczek, F.; Berndt, R. Electron-Induced Spin Crossover of Single Molecules in a Bilayer on Gold. *Angew. Chem., Int. Ed.* **2012**, *51*, 6262−6266.

(10) Schäfer, B.; Rajnák, C.; Šalitroš, I.; Fuhr, O.; Klar, D.; Schmitz-Antoniak, C.; Weschke, E.; Wende, H.; Ruben, M. Room Temperature Switching of a Neutral Molecular Iron(ii) Complex. *Chem. Commun.* **2013**, *49*, 10986−10988.

(11) Shi, S.; Schmerber, G.; Arabski, J.; Beaufrand, J.-B.; Kim, D. J.; Boukari, S.; Bowen, M.; Kemp, N. T.; Viart, N.; Rogez, G.; et al. Study of Molecular Spin-Crossover Complex Fe(phen)$_2$(NCS)$_2$ Thin Films. *Appl. Phys. Lett.* **2009**, *95*, 043303.

(12) Mahfoud, T.; Molnár, G.; Cobo, S.; Salmon, L.; Thibault, C.; Vieu, C.; Demont, P.; Bousseksou, A. Electrical Properties and Non-Volatile Memory Effect of the $[Fe(HB(pz)_3)_2]$ Spin Crossover Complex Integrated in a Microelectrode Device. *Appl. Phys. Lett.* **2011**, *99*, 053307.

(13) Bernien, M.; Wiedemann, D.; Hermanns, C. F.; Krüger, A.; Rolf, D.; Kroener, W.; Müller, P.; Grohmann, A.; Kuch, W. Spin Crossover in a Vacuum-Deposited Submonolayer of a Molecular Iron(II) Complex. *J. Phys. Chem. Lett.* **2012**, *3*, 3431–3434.

(14) Lefter, C.; Rat, S.; Costa, J. S.; Manrique-Juárez, M. D.; Quintero, C. M.; Salmon, L.; Séguy, I.; Leichle, T.; Nicu, L.; Demont, P.; et al. Current Switching Coupled to Molecular Spin-States in Large-Area Junctions. *Adv. Mater.* **2016**, *28*, 7508–7514.

(15) Bairagi, K.; Iasco, O.; Bellec, A.; Kartsev, A.; Li, D.; Lagoute, J.; Chacon, C.; Girard, Y.; Rousset, S.; Miserque, F.; et al. Molecular-Scale Dynamics of Light-Induced Spin Cross-over in a Two-Dimensional Layer. *Nat. Commun.* **2016**, *7*, 12212.

(16) Davesne, V.; Gruber, M.; Studniarek, M.; Doh, W. H.; Zafeiratos, S.; Joly, L.; Sirotti, F.; Silly, M. G.; Gaspar, A. B.; Real, J. A.; et al. Hysteresis and Change of Transition Temperature in Thin Films of Fe{[Me$_2$Pyrz]$_3$BH}$_2$, a New Sublimable Spin-Crossover Molecule. *J. Chem. Phys.* **2015**, *142*, 194702.

(17) Real, J. A.; Muñoz, M. C.; Faus, J.; Solans, X. Spin Crossover in Novel Dihydrobis(1-Pyrazolyl)borate [H$_2$B(pz)$_2$]-Containing Iron(II) Complexes. Synthesis, X-Ray Structure, and Magnetic Properties of [FeL{H$_2$B(pz)$_2$}$_2$] (L = 1,10-Phenanthroline and 2,2′-Bipyridine). *Inorg. Chem.* **1997**, *36*, 3008–3013.

(18) Moliner, N.; Salmon, L.; Capes, L.; Muñoz, M. C.; Létard, J.-F.; Bousseksou, A.; Tuchagues, J.-P.; McGarvey, J. J.; Dennis, A. C.; Castro, M.; et al. Thermal and Optical Switching of Molecular Spin States in the {[FeL[H$_2$B(pz)$_2$]$_2$} Spin-Crossover System (L = Bpy, Phen). *J. Phys. Chem. B* **2002**, *106*, 4276–4283.

(19) Thompson, A. L.; Goeta, A. E.; Real, J. A.; Galet, A.; Carmen Muñoz, M. Thermal and Light Induced Polymorphism in Iron(ii) Spin Crossover Compounds. *Chem. Commun.* **2004**, *12*, 1390–1391.

(20) Galet, A.; Gaspar, A. B.; Agusti, G.; Muñoz, M. C.; Levchenko, G.; Real, J. A. Pressure Effect Investigations on the Spin Crossover Systems{Fe[H$_2$B(pz)$_2$]$_2$(bipy)} and {Fe[H$_2$B(pz)$_2$]$_2$(phen)}. *Eur. J. Inorg. Chem.* **2006**, *2006*, 3571–3573.

(21) Naggert, H.; Bannwarth, A.; Chemnitz, S.; von Hofe, T.; Quandt, E.; Tuczek, F. First Observation of Light-Induced Spin Change in Vacuum Deposited Thin Films of Iron Spin Crossover Complexes. *Dalton Trans.* **2011**, *40*, 6364–6366.

(22) Palamarciuc, T.; Oberg, J. C.; El Hallak, F.; Hirjibehedin, C. F.; Serri, M.; Heutz, S.; Létard, J.-F.; Rosa, P. Spin Crossover Materials Evaporated under Clean High Vacuum and Ultra-High Vacuum Conditions: From Thin Films to Single Molecules. *J. Mater. Chem.* **2012**, *22*, 9690–9695.

(23) Ludwig, E.; Naggert, H.; Kalläne, M.; Rohlf, S.; Kröger, E.; Bannwarth, A.; Quer, A.; Rossnagel, K.; Kipp, L.; Tuczek, F. Iron(II) Spin-Crossover Complexes in Ultrathin Films: Electronic Structure and Spin-State Switching by Visible and Vacuum-UV Light. *Angew. Chem., Int. Ed.* **2014**, *53*, 3019–3023.

(24) Zhang, X.; Palamarciuc, T.; Rosa, P.; Létard, J.-F.; Doudin, B.; Zhang, Z.; Wang, J.; Dowben, P. A. Electronic Structure of a Spin Crossover Molecular Adsorbate. *J. Phys. Chem. C* **2012**, *116*, 23291–23296.

(25) Pronschinske, A.; Bruce, R. C.; Lewis, G.; Chen, Y.; Calzolari, A.; Buongiorno-Nardelli, M.; Shultz, D. A.; You, W.; Dougherty, D. B. Iron(ii) Spin Crossover Films on Au(111): Scanning Probe Microscopy and Photoelectron Spectroscopy. *Chem. Commun.* **2013**, *49*, 10446–10452.

(26) Pronschinske, A.; Chen, Y.; Lewis, G. F.; Shultz, D. A.; Calzolari, A.; Buongiorno Nardelli, M.; Dougherty, D. B. Modification of Molecular Spin Crossover in Ultrathin Films. *Nano Lett.* **2013**, *13*, 1429–1434.

(27) Warner, B.; Oberg, J. C.; Gill, T. G.; El Hallak, F.; Hirjibehedin, C. F.; Serri, M.; Heutz, S.; Arrio, M.-A.; Sainctavit, P.; Mannini, M.; et al. Temperature- and Light-Induced Spin Crossover Observed by X-Ray Spectroscopy on Isolated Fe(II) Complexes on Gold. *J. Phys. Chem. Lett.* **2013**, *4*, 1546–1552.

(28) Zhang, X.; Palamarciuc, T.; Letard, J.-F.; Rosa, P.; Lozada, E. V.; Torres, F.; Rosa, L. G.; Doudin, B.; Dowben, P. A. The Spin State of a Molecular Adsorbate Driven by the Ferroelectric Substrate Polarization. *Chem. Commun.* **2014**, *50*, 2255–2257.

(29) Zhang, X.; Mu, S.; Chastanet, G.; Daro, N.; Palamarciuc, T.; Rosa, P.; Létard, J.-F.; Liu, J.; Sterbinsky, G. E.; Arena, D. A.; et al. Complexities in the Molecular Spin Crossover Transition. *J. Phys. Chem. C* **2015**, *119*, 16293–16302.

(30) Gentili, D.; Liscio, F.; Demitri, N.; Schafer, B.; Borgatti, F.; Torelli, P.; Gobaut, B.; Panaccione, G.; Rossi, G.; Degli Esposti, A.; et al. Surface Induces Different Crystal Structures in a Room Temperature Switchable Spin Crossover Compound. *Dalton Trans.* **2016**, *45*, 134–143.

(31) Gopakumar, T. G.; Bernien, M.; Naggert, H.; Matino, F.; Hermanns, C. F.; Bannwarth, A.; Mühlenberend, S.; Krüger, A.; Krüger, D.; Nickel, F.; et al. Spin-Crossover Complex on Au(111): Structural and Electronic Differences Between Mono- and Multilayers. *Chem. - Eur. J.* **2013**, *19*, 15702–15709.

(32) Bernien, M.; Naggert, H.; Arruda, L. M.; Kipgen, L.; Nickel, F.; Miguel, J.; Hermanns, C. F.; Krüger, A.; Krüger, D.; Schierle, E.; et al. Highly Efficient Thermal and Light-Induced Spin-State Switching of an Fe(II) Complex in Direct Contact with a Solid Surface. *ACS Nano* **2015**, *9*, 8960–8966.

(33) Beniwal, S.; Zhang, X.; Mu, S.; Naim, A.; Rosa, P.; Chastanet, G.; Létard, J.-F.; Liu, J.; Sterbinsky, G. E.; Arena, D. A.; et al. Surface-Induced Spin State Locking of the [Fe(H 2 B(pz) 2) 2 (Bipy)] Spin Crossover Complex. *J. Phys.: Condens. Matter* **2016**, *28*, 206002.

(34) Bronner, C.; Priewisch, B.; Rück-Braun, K.; Tegeder, P. Photoisomerization of an Azobenzene on the Bi(111) Surface. *J. Phys. Chem. C* **2013**, *117*, 27031–27038.

(35) Schulze, G.; Franke, K. J.; Pascual, J. I. Induction of a Photostationary Ring-Opening—Ring-Closing State of Spiropyran Monolayers on the Semimetallic Bi(110) Surface. *Phys. Rev. Lett.* **2012**, *109*, 026102.

(36) Naggert, H.; Rudnik, J.; Kipgen, L.; Bernien, M.; Nickel, F.; Arruda, L. M.; Kuch, W.; Näther, C.; Tuczek, F. Vacuum-Evaporable Spin-Crossover Complexes: Physicochemical Properties in the Crystalline Bulk and in Thin Films Deposited from the Gas Phase. *J. Mater. Chem. C* **2015**, *3*, 7870–7877.

(37) Rudnik, J.; Naggert, H.; Schwarzer, S.; Tuczek, F.; Parchmann, I. "Künstliches Blut" — Synthese eines magnetisch und farblich schaltbaren Eisen-Komplexes. *CHEMKON* **2014**, *21*, 85–88.

(38) Kulmaczewski, R.; Shepherd, H. J.; Cespedes, O.; Halcrow, M. A. A Homologous Series of [Fe(H$_2$Bpz$_2$)$_2$(L)] Spin-Crossover Complexes with Annelated Bipyridyl Co-Ligands. *Inorg. Chem.* **2014**, *53*, 9809–9817.

(39) Nihei, M.; Suzuki, Y.; Kimura, N.; Kera, Y.; Oshio, H. Bidirectional Photomagnetic Conversions in a Spin-Crossover Complex with a Diarylethene Moiety. *Chem. - Eur. J.* **2013**, *19*, 6946–6949.

(40) Milek, M.; Heinemann, F. W.; Khusniyarov, M. M. Spin Crossover Meets Diarylethenes: Efficient Photoswitching of Magnetic Properties in Solution at Room Temperature. *Inorg. Chem.* **2013**, *52*, 11585–11592.

(41) Rösner, B.; Milek, M.; Witt, A.; Gobaut, B.; Torelli, P.; Fink, R. H.; Khusniyarov, M. M. Reversible Photoswitching of a Spin-Crossover Molecular Complex in the Solid State at Room Temperature. *Angew. Chem., Int. Ed.* **2015**, *54*, 12976–12980.

(42) Katayama, K.; Hirotsu, M.; Kinoshita, I.; Teki, Y. Design, Synthesis, Magnetic Properties of a π-Radical Ligand with Photo-Excited High-Spin State and Its Fe(II) Complex. The First Stage of a New Strategy for LIESST Materials. *Dalton Trans.* **2012**, *41*, 13465–13473.

(43) Decurtins, S.; Gütlich, P.; Köhler, C. P.; Spiering, H.; Hauser, A. Light-Induced Excited Spin State Trapping in a Transition-Metal Complex: The Hexa-1-Propyltetrazole-Iron (II) Tetrafluoroborate Spin-Crossover System. *Chem. Phys. Lett.* **1984**, *105*, 1–4.

(44) Hauser, A. Light-Induced Spin Crossover and the High-Spin→ Low-Spin Relaxation. In *Spin Crossover in Transition Metal Compounds II*; Topics in Current Chemistry 234; Springer: Berlin, 2004; pp 155–198.

(45) Cartier dit Moulin, C.; Rudolf, P.; Flank, A. M.; Chen, C. Te. Spin Transition Evidenced by Soft X-Ray Absorption Spectroscopy. *J. Phys. Chem.* **1992**, *96*, 6196−6198.

(46) Collison, D.; Garner, C. D.; McGrath, C. M.; Mosselmans, J. F. W.; Roper, M. D.; Seddon, J. M. W.; Sinn, E.; Young, N. A. Soft X-Ray Induced Excited Spin State Trapping and Soft X-Ray Photochemistry at the Iron $L_{2,3}$ Edge in $[Fe(phen)_2(NCS)_2]$ and $[Fe(phen)_2(NCSe)_2]$ (Phen = 1,10-Phenanthroline). *J. Chem. Soc., Dalton Trans.* **1997**, *22*, 4371−4376.

(47) Jesson, J. P.; Trofimenko, S.; Eaton, D. R. Spectra and Structure of Some Transition Metal poly(1-Pyrazolyl) Borates. *J. Am. Chem. Soc.* **1967**, *89*, 3148−3158.

(48) Stöhr, J.; Outka, D. A. Determination of Molecular Orientations on Surfaces from the Angular Dependence of near-Edge X-Ray-Absorption Fine-Structure Spectra. *Phys. Rev. B: Condens. Matter Mater. Phys.* **1987**, *36*, 7891−7905.

(49) Rodriguez-Reyes, J. C. F.; Siler, C. G. F.; Liu, W.; Tkatchenko, A.; Friend, C. M.; Madix, R. J. Van Der Waals Interactions Determine Selectivity in Catalysis by Metallic Gold. *J. Am. Chem. Soc.* **2014**, *136*, 13333−13340.

(50) Hauser, A.; Spiering, H.; Schollmeyer, D.; Gütlich, P.; Hinek, R. The $[Fe(etz)_6](BF_4)_2$ Spin-Crossover System—Part One: High-Spin ⇌ Low-Spin Transition in Two Lattice Sites. *Chem. - Eur. J.* **1996**, *2*, 1427−1434.

(51) Trofimenko, S. Boron-Pyrazole Chemistry. II. Poly(1-Pyrazolyl)-Borates. *J. Am. Chem. Soc.* **1967**, *89*, 3170−3177.

(52) Becke, A. D. Density-functional Thermochemistry. III. The Role of Exact Exchange. *J. Chem. Phys.* **1993**, *98*, 5648−5652.

(53) Lee, C.; Yang, W.; Parr, R. G. Development of the Colle-Salvetti Correlation-Energy Formula into a Functional of the Electron Density. *Phys. Rev. B: Condens. Matter Mater. Phys.* **1988**, *37*, 785−789.

(54) Stephens, P. J.; Devlin, F. J.; Chabalowski, C. F.; Frisch, M. J. Ab Initio Calculation of Vibrational Absorption and Circular Dichroism Spectra Using Density Functional Force Fields. *J. Phys. Chem.* **1994**, *98*, 11623−11627.

(55) McLean, A. D.; Chandler, G. S. Contracted Gaussian Basis Sets for Molecular Calculations. I. Second Row Atoms, Z = 11−18. *J. Chem. Phys.* **1980**, *72*, 5639.

(56) Krishnan, R.; Binkley, J. S.; Seeger, R.; Pople, J. A. Self-consistent Molecular Orbital Methods. XX. A Basis Set for Correlated Wave Functions. *J. Chem. Phys.* **1980**, *72*, 650.

(57) Blaudeau, J.-P.; McGrath, M. P.; Curtiss, L. A.; Radom, L. Extension of Gaussian-2 (G2) Theory to Molecules Containing Third-Row Atoms K and Ca. *J. Chem. Phys.* **1997**, *107*, 5016.

(58) Wachters, A. J. H. Gaussian Basis Set for Molecular Wavefunctions Containing Third-Row Atoms. *J. Chem. Phys.* **1970**, *52*, 1033.

(59) Hay, P. J. Gaussian Basis Sets for Molecular Calculations. The Representation of 3d Orbitals in Transition-metal Atoms. *J. Chem. Phys.* **1977**, *66*, 4377.

(60) Binning, R. C.; Curtiss, L. A. Compact Contracted Basis Sets for Third-Row Atoms: Ga−Kr. *J. Comput. Chem.* **1990**, *11*, 1206−1216.

(61) McGrath, M. P.; Radom, L. Extension of Gaussian-1 (G1) Theory to Bromine-containing Molecules. *J. Chem. Phys.* **1991**, *94*, 511.

(62) Curtiss, L. A.; McGrath, M. P.; Blaudeau, J.; Davis, N. E.; Binning, R. C.; Radom, L. Extension of Gaussian-2 Theory to Molecules Containing Third-row Atoms Ga−Kr. *J. Chem. Phys.* **1995**, *103*, 6104.

(63) Tao, J.; Perdew, J. P.; Staroverov, V. N.; Scuseria, G. E. Climbing the Density Functional Ladder: Nonempirical Meta-Generalized Gradient Approximation Designed for Molecules and Solids. *Phys. Rev. Lett.* **2003**, *91*, 146401.

(64) Schäfer, A.; Horn, H.; Ahlrichs, R. Fully Optimized Contracted Gaussian Basis Sets for Atoms Li to Kr. *J. Chem. Phys.* **1992**, *97*, 2571−2577.

(65) Schäfer, A.; Huber, C.; Ahlrichs, R. Fully Optimized Contracted Gaussian Basis Sets of Triple Zeta Valence Quality for Atoms Li to Kr. *J. Chem. Phys.* **1994**, *100*, 5829−5835.

(66) Frisch, M. J.; Trucks, G. W.; Schlegel, H. B.; Scuseria, G. E.; Robb, M. A.; Cheeseman, J. R.; Montgomery, J. A., Jr.; Vreven, T.; Kudin, K. N.; Burant, J. C.; et al. *Gaussian 09*, revision D.01; Gaussian, Inc.: Wallingford, CT, 2009.

(67) Mayo, S. L.; Olafson, B. D.; Goddard, W. A. DREIDING: A Generic Force Field for Molecular Simulations. *J. Phys. Chem.* **1990**, *94*, 8897−8909.